Acta Crystallographica Section B
Structural Science
ISSN 0108-7681

Polymorphism in the spin-crossover ferric complexes [(TPA)Fe^{III}(TCC)]PF_6

Eric Collet,[a]* Marie-Laure Boillot,[b] Johan Hebert,[a] Nicolas Moisan,[a] Marina Servol,[a] Maciej Lorenc,[a] Loïc Toupet,[a] Marylise Buron-Le Cointe,[a] Antoine Tissot[b] and Joelle Sainton[b]

[a]Institut de Physique de Rennes, UMR-CNRS 6251, Université de Rennes 1 35042 Rennes CEDEX, France, and [b]Institut de Chimie Moléculaire et des Matériaux d'Orsay, UMR-CNRS 8182, Université Paris-Sud, Orsay, France

Correspondence e-mail: eric.collet@univ-rennes1.fr

Received 27 March 2009
Accepted 5 June 2009

We have identified two polymorphs of the molecular complex [(TPA)$Fe^{(III)}$(TCC)]PF_6 [TPA = tris(2-pyridylmethyl)amine and TCC = 3,4,5,6-tetrachlorocatecholate dianion]: one is monoclinic and the other is orthorhombic. By lowering the temperature both undergo a thermal spin-crossover between a high-spin (S = 5/2) and a low-spin (S = 1/2) state, which we detected by magnetic, optical and X-ray diffraction measurements. The thermal crossover is only slightly shifted between the polymorphs. Their crystalline structures consist of similar cation layers alternating with PF_6 anion layers, packed differently in the two polymorphs. The magnetic and optical properties of the polymorphs are presented.

1. Introduction

Spin-crossover molecular solids can change their magnetic response under the influence of stimuli of different nature such as temperature, pressure and light irradiation. The spin crossover may occur between the low-spin (LS) and the high-spin (HS) states (Gütlich & Goodwin, 2004) of $3d^4$–$3d^7$ transition-metal ions in pseudo-octahedral complexes. In the iron(III) derivatives investigated here, the LS (S = 1/2) and HS (S = 5/2) states are both paramagnetic (Koningsbruggen *et al.*, 2004). Such spin conversions have been observed for molecules in solution and in the solid state, as well as in newly developed nanoscale molecular objects (Duriska *et al.*, 2009). However, in solids the thermal spin conversion may drastically change between the different polymorphs from a crossover (gradual spin-state conversion) to a first-order transition (discontinuous variation of the HS fraction), as in the case of Fe^{II}-(PM-BIA)$_2$(NCS)$_2$ for example (Létard *et al.*, 1998, 2003; Marchivie *et al.*, 2003). In some extreme cases one of the polymorphs shows a thermal conversion, whereas the other does not (Mitra *et al.*, 1978; Matouzenko *et al.*, 1997; Thompson *et al.*, 2004; Reger *et al.*, 2005; Sheu *et al.*, 2008). Studying polymorphism is therefore important for a better understanding of the relative intra- and intermolecular contributions to the spin conversion. In this paper we report an experimental comparison of the spin-crossover properties of two polymorphs of the ferric catecholate complex [(TPA)Fe(TCC)]PF_6 [Fig. 1; TPA = tris(2-pyridylmethyl)-amine and TCC = 3,4,5,6-tetrachlorocatecholate dianion]. One is orthorhombic (1) (Floquet *et al.*, 2005) and the new one is monoclinic (2). The electronic properties of this family of complexes are related to some quantum mixing between two configurations of Fe^{III} catecholate and Fe^{II} semiquinonate (Simaan *et al.*, 2005). The electronic delocalization occurring between the dioxolene and the metal centre is directly modulated by the catecholate substituent, here chlorine atoms (Girerd *et al.*, 2008). Absorption spectra provide clear

evidence of both the electronic effect in the high-spin and the low-spin states, and the spin crossover (Enachescu *et al.*, 2006). The unusual feature of this study is that the thermal spin conversions of (1) and (2) are very similar, in contrast to earlier reports on other spin-crossover polymorphs, while the optical spectra are different. Here we present temperature-dependent investigations of both polymorphs by using magnetic and optical measurements, as well as single-crystal X-ray diffraction. The results are discussed in relation to the Ising-like model of the spin-crossover phenomenon.

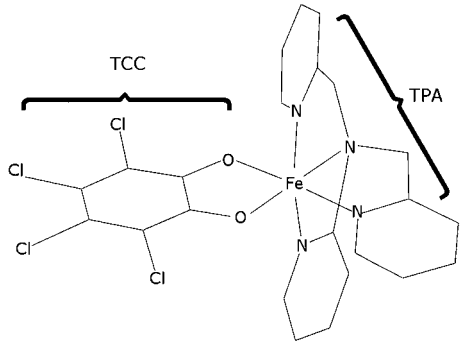

2. Experimental

The [(TPA)Fe(TCC)]PF_6 complex was synthesized as previously described (Floquet *et al.*, 2005). Single crystals were obtained from powder dissolved either in an acetone/MeOH (1) or an MeOH/H_2O (2) mixture ($\sim$ 1/9 for the former and 9/1 for the latter). Deep purple platelets [orthorhombic polymorph (1)] or thin orange needles [monoclinic polymorph (2)] of [(TPA)Fe(TCC)]PF_6 were isolated by filtration from (1) and (2) solutions (Fig. 2). Magnetic susceptibility measurements were carried out with a Quantum Design SQUID Magnetometer (Model MPMS5S) calibrated against a palladium standard. The measurements were performed on crystalline samples (single crystals which have been carefully reduced in size). No anisotropic effect was detected, in particular at low temperature. The fraction of HS molecules X_{HS} was estimated from the $\chi_m T$ product (χ_m = molar magnetic susceptibility) as the weighted contribution of molecules in the HS and in the LS states

$$\chi_m T = X_{HS}(T)(\chi_m T)_{HS} + (1 - X_{HS}(T))(\chi_m T)_{LS}, \qquad (1)$$

where $(\chi_m T)_{HS}$ = 4.375 cm^3 mol^{-1} K for S = 5/2, $(\chi_m T)_{LS} \simeq (1/8)g^2[S(S+1)]$ = 0.43 cm^3 mol^{-1} K for S = 1/2 and g = 2.11–2.15 from the LS electron paramagnetic resonance spectra (EPR, solution and solids).

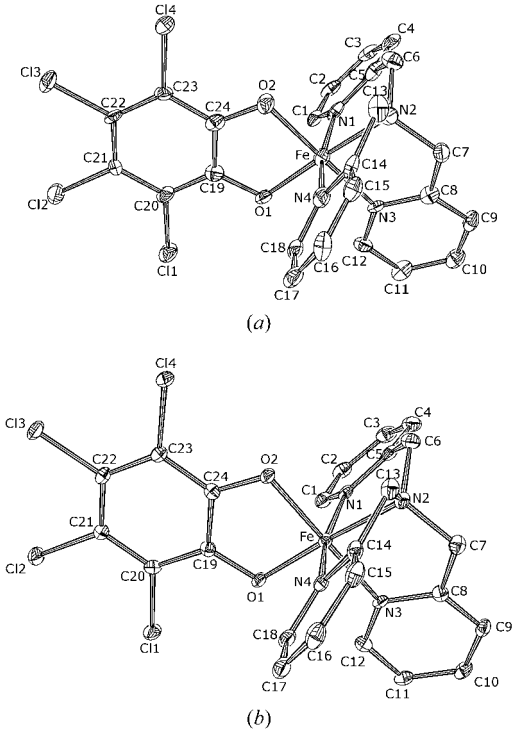

Figure 1
ORTEP (Johnson, 1965; Farrugia, 1997) view of the molecular structures of the (*a*) orthorhombic and (*b*) monoclinic polymorphs at 80 K. Displacement ellipsoids are at the 50% level.

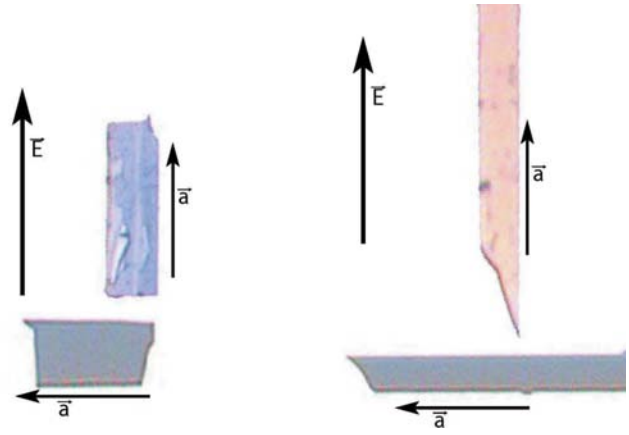

Figure 2
The two types of polymorphs of the [(TPA)Fe(TCC)]PF_6 complex: the orthorhombic (left) and monoclinic (right) forms. For both, the *b* axis is perpendicular to the plane of the figure and *E* corresponds to the polarization of light.

Photographs of $\sim$ 10 µm thick single crystals of both polymorphs were taken in transmission mode on a Laborlux 12 pol standard optical microscope from Leica equipped with a Sony Digital Hyper HAD SSC-DC38P CCD camera. Optical transmission experiments were performed at 480 and 600 nm to characterize the thermal conversion of both compounds. We used light polarized parallel to the long crystal axis (crystallographic axis *a*), which yields maximum transmission.

X-ray diffraction experiments were performed on single crystals of both polymorphs on an Xcalibur 3 diffractometer (Oxford Diffraction) at different temperatures. The crystals were mounted in an Oxford Cryosystems nitrogen-flow cryostat. The unit-cell parameters and data reduction were obtained with *CrysAlis* software (Oxford Diffraction, 2008*a*,*b*). Structures were solved with *SIR*97 (Altomare *et al.*, 1999) and refined with *SHELXL*97 (Sheldrick, 2008). Comparison of the structural parameters for both polymorphs

Table 1
Crystal data and structure refinement for the orthorhombic and monoclinic polymorphs in the HS and LS states.

	Monoclinic (80 K)	Orthorhombic (80 K)	Monoclinic (400 K)	Orthorhombic (400 K)
Crystal data				
Chemical formula	$C_{24}H_{18}Cl_4F_6FeN_4O_2P$	$C_{24}H_{18}Cl_4F_6FeN_4O_2P$	$C_{24}H_{18}Cl_4F_6FeN_4O_2P$	$C_{24}H_{18}Cl_4F_6FeN_4O_2P$
M_r	737.04	737.04	737.04	737.04
Crystal system, space group	Monoclinic, $P2_1/a$	Orthorhombic, $Pna2_1$	Monoclinic, $P2_1/a$	Orthorhombic, $Pna2_1$
Temperature (K)	80	80	400	400
a, b, c (Å)	8.4250 (2), 35.9730 (8), 9.0586 (2)	8.3086 (2), 36.1529 (8), 9.1975 (2)	8.6788 (6), 37.001 (2), 9.2881 (5)	8.561 (2), 37.414 (9), 9.452 (2)
β (°)	91.942 (2)	90.00	91.255 (2)	90.00
V (Å^3)	2743.84 (11)	2762.74 (11)	2981.9 (3)	3027.5 (12)
Z	4	4	4	4
Radiation type	Mo $K\alpha$	Mo $K\alpha$	Mo $K\alpha$	Mo $K\alpha$
μ (mm^{-1})	1.07	1.06	0.99	0.97
Crystal form, size (mm)	Needle, 0.25 × 0.05 × 0.05	Plate, 0.20 × 0.20 × 0.05	Needle, 0.25 × 0.05 × 0.05	Plate, 0.20 × 0.20 × 0.05
Data collection				
Diffractometer	CCD Sapphire 3 Xcalibur	CCD Sapphire 3 Xcalibur	CCD Sapphire 3 Xcalibur	CCD Sapphire 3 Xcalibur
Data collection method	ω scans	ω scans	ω scans	ω scans
Absorption correction	None	None	None	None
No. of measured, independent and observed reflections	36 645, 5983, 4967	34 420, 5992, 4026	38 192, 5982, 1817	35 296, 6576, 1760
Criterion for observed reflections	$I > 2\sigma(I)$	$I > 2\sigma(I)$	$I > 2\sigma(I)$	$I > 2\sigma(I)$
R_{int}	0.040	0.091	0.123	0.121
θ_{max} (°)	27.0	27.0	27.0	27.0
Refinement				
Refinement on	F^2	F^2	F^2	F^2
$R[F^2 > 2\sigma(F^2)]$, $wR(F^2)$, S	0.054, 0.109, 1.20	0.041, 0.068, 0.80	0.046, 0.124, 0.71	0.037, 0.100, 0.53
No. of reflections	5983	5992	5982	6576
No. of parameters	379	379	379	379
H-atom treatment	Constrained†	Constrained†	Constrained†	Constrained†
$(\Delta/\sigma)_{max}$	< 0.0001	0.001	< 0.0001	0.001
$\Delta\rho_{max}$, $\Delta\rho_{min}$ (e Å^{-3})	0.67, −0.76	0.71, −0.45	0.35, −0.31	0.31, −0.24

Computer programs used: *CrysAlis CCD* (Oxford Diffraction, 2008*a*), *CrysAlis RED* (Oxford Diffraction, 2008*b*), *SIR*97 (Altomare *et al.*, 1999), *SHELXL*97 (Sheldrick, 2008), *PLATON* (Spek, 2009). † Constrained to parent site.

in the HS (400 K) and LS (80 K) states is presented in Table 1. Several data sets were collected at 400 and 80 K for both polymorphs. The results in Tables 1 and 2 correspond to the measurements with the best R_{int}.

3. Results

3.1. Magnetic studies

The temperature dependence of the $\chi_M T$ product (molar magnetic susceptibility times temperature) for polymorphs (1) and (2) is shown in Fig. 3. Both undergo a gradual thermal crossover from the high-temperature HS state to the low-temperature LS one. The magnetic response values of both polymorphs observed in the high-temperature regime are similar and approach the limit expected for the S = 5/2 spin state ($\chi_m T$ = 4.375 cm^3 mol^{-1} K). At low temperatures, the values correspond well with those expected for S = 1/2 (g = 2.11–2.15, $\chi_m T$ = 0.43 cm^3 mol^{-1} K). Estimations of the characteristic temperatures $T_{1/2}$ (corresponding to 50% conversion of the metal ions and therefore to $\chi_m T$ = 2.403 cm^3 mol^{-1} K) give slightly different values: $T_{1/2} \simeq 214$ K for the new monoclinic system, which is up-shifted by ~ 11 K from the orthorhombic system.

3.2. Optical transmission

The photographs obtained with the microscope in transmission mode gave differently coloured crystals in the HS

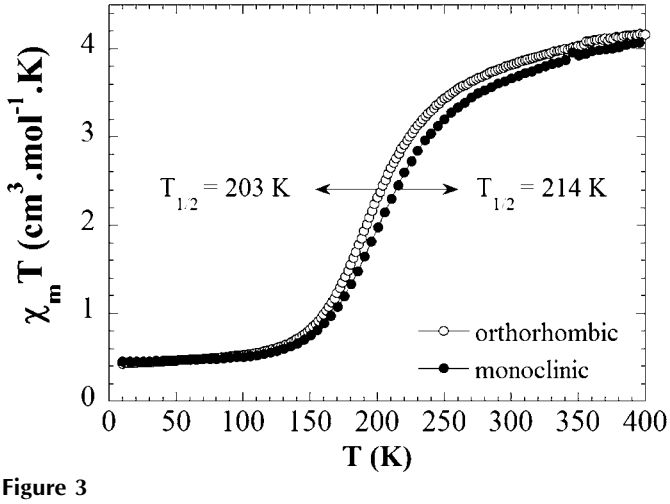

Figure 3
$\chi_m T$ *versus* temperature for the monoclinic and orthorhombic polymorphs.

[1] Supplementary data for this paper are available from the IUCr electronic archives (Reference: OG5037). Services for accessing these data are described at the back of the journal.

Table 2
The geometry of the Fe site surroundings.

	Monoclinic HS 400 K	Monoclinic LS 80 K	Orthorhombic HS 400 K	Orthorhombic LS 80 K
C—O bonds (Å)				
O1—C19	1.335 (5)	1.333 (4)	1.353 (7)	1.350 (6)
O2—C24	1.337 (5)	1.320 (4)	1.340 (7)	1.326 (6)
Fe—N bonds (Å)				
Fe—N1	2.111 (5)	1.967 (3)	2.118 (6)	1.954 (5)
Fe—N2	2.175 (4)	1.996 (3)	2.183 (4)	1.998 (4)
Fe—N3	2.105 (4)	1.949 (3)	2.127 (5)	1.933 (4)
Fe—N4	2.116 (4)	1.954 (3)	2.114 (5)	1.964 (5)
⟨Fe—N⟩	2.127 (8)	1.967 (3)	2.135 (5)	1.962 (4)
Fe—O bonds (Å)				
Fe—O1	1.924 (6)	1.857 (3)	1.928 (3)	1.862 (3)
Fe—O2	1.928 (6)	1.928 (3)	1.945 (3)	1.917 (3)
⟨Fe—O⟩	1.926 (6)	1.893 (4)	1.936 (3)	1.890 (3)
ζ (Å)	0.53 (2)	0.20 (1)	0.53 (1)	0.20 (1)
Σ (°)	88 (4)	49 (2)	86 (2)	49 (2)

$\zeta = \sum_{i=1}^{6} |\text{Fe}-L_i - \langle \text{Fe}-L \rangle|$ and $\Sigma = \sum_{i=1}^{12} |90 - \phi_i|$.

state (purple for the orthorhombic polymorph and orange for the monoclinic polymorph, Fig. 2). When light is polarized along the *c* axis the transmission through 15 µm thick crystals is too weak for detection. The change of colour related to polymorphism has already been reported in different types of systems. It may originate from different conformations of molecular structures (Yu, 2002), but also from the crystal packing itself, which may modify π–π overlap for example (Peresypkina *et al.*, 2005).

The thermal evolution is also different for the two polymorphs (Fig. 4). The transmission in the visible range is lower in the HS state for the orthorhombic polymorph: the optical density (OD) increases between the LS and HS states as the colour changes from light blue to dark blue, as plotted at 480 and 600 nm (Fig. 4). For the monoclinic polymorph, the OD at 600 nm decreases, whereas it increases at 480 nm. The sample colour changes from dark violet in the LS state to orange in the HS one. In both cases this thermochromism occurs around the crossover temperatures as it results from the change of spin state. A similar variation in optical properties related to the spin state was used to demonstrate the possibility of generating transient spin-state trapping within a ms lifetime with laser pulse (Enachescu *et al.*, 2006; Moisan *et al.*, 2008).

3.3. Structural changes

In order to understand the differences between the two types of crystals, X-ray diffraction was performed at different temperatures. Structures were solved with the $Pna2_1$ space group for the orthorhombic form (1) in agreement with Floquet *et al.* (2005), whereas the $P2_1/a$ space group was chosen for the new monoclinic (2) form. This choice allowed the same *ac* plane in both polymorphs to remain. The *ORTEP* (Johnson, 1965) view of the cation structure of both polymorphs is presented in Fig. 1 and details of the structural analysis are presented in Tables 1 and 2.

The strong coupling between the electronic and structural degrees of freedom is characterized by a significant reorganization of the crystalline structure at the intra- and intermolecular levels, as already observed during several structural studies of different systems undergoing thermal conversions (Marchivie *et al.*, 2003; Guionneau *et al.*, 2004) or photo-induced spin conversions (Collet *et al.*, 2008; Pillet *et al.*, 2008; Glijer *et al.*, 2008). Important structural changes occur at the level of the coordination sphere surrounding the Fe atom. The thermal dependence of the average ⟨Fe—N⟩ bond length, derived from the structural analysis, is similar for both compounds (Table 2). It corresponds to a typical 0.16 Å bond contraction associated with the HS to LS state conversion, as the bonding character of the electronic distribution is stronger in the LS state (Guionneau *et al.*, 2004). The Fe—O contraction is smaller [0.05 Å for (1) and 0.03 Å for (2)]. The deformation of the octahedron surrounding the Fe site is another clear signature of the spin state. For a quantitative characterization, the parameter Σ was introduced (Marchivie *et al.*, 2003), which is the sum of deviations from 90° of the 12 *cis* φ_i angles in the coordination sphere (Table 2). For both polymorphs Σ decreases from $\sim$ 87° in the HS state down to $\sim$ 49 ° in the LS state. Another deformation is characterized by the ζ parameter (Table 2), which is a measure of deviation from the average distance between the central Fe atom and its nearest neighbours L_i (O or N). Here again it is less significant in the LS state than in the HS state. Therefore, the [FeL_6] octahedron is more regular for the LS state of both polymorphs, as usually observed in spin-crossover materials (Guionneau *et al.*, 2004).

Although the average environment of the Fe atom is rather similar in both polymorphs, and in particular the ⟨Fe—N⟩ bond lengths, there are still differences upon closer inspection of the crystallographic data (CIF files and Fig. 1). These discrepancies between orthorhombic and monoclinic forms first concern two bond angles N1—Fe—N3 [86.37 (13) for (1)

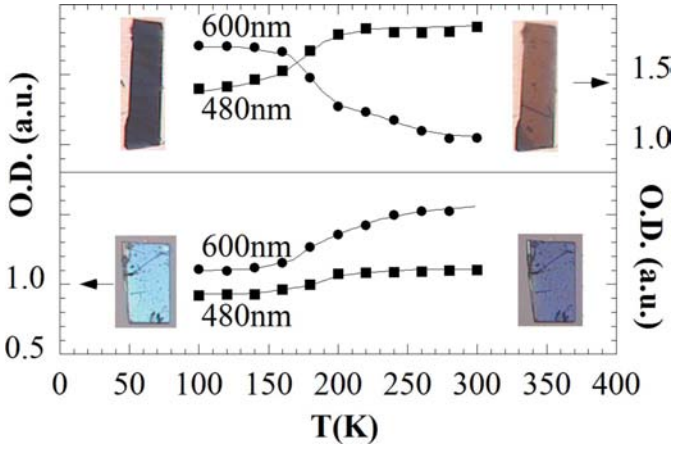

Figure 4
Temperature dependence of the crystal colours and optical densities (OD) at 480 and 600 nm for the orthorhombic (bottom) and monoclinic (top) polymorphs. Measurements were performed with light parallel polarized to the long crystal axis *a*. Photographs were obtained at 50 and 350 K.

and 92.22 (13) for (2) at 80 K] and N3—Fe—N4 [93.33 (15) for (1) and 87.34 (12) for (2) at 80 K] and their different variations during the thermal crossover from LS (80 K) to HS (400 K) states. These angular changes indicate specific reorganization in the tetradentate TPA ligand for each polymorph. In addition, the mean ⟨C—O⟩ bond length is smaller for molecules in the monoclinic solid [at 80 (400) K, 1.331 (1.346) Å and 1.326 (1.336) Å, for (1) and (2) respectively]. This observation holds at any temperature, despite some variations related to the crossover. In the literature, the C—O bond of the dioxolene-iron(III) moiety markedly depends on the redox isomer: 1.35–1.37 Å for Fe^{III} catecholate (Jang *et al.*, 1991; Jo & Que, 2000) and 1.27–1.29 Å for Fe^{III} semiquinonate (Koch *et al.*, 1998; Boone *et al.*, 1989). The electronic state of the catecholate moiety is discussed in relation to the C—O bond length, which varies with the electronic state, while the ring's C—C bond lengths also depend on the nature of the catechol substituent (Floquet *et al.*, 2005). The C—C bonds of the TCC cycles are equal within the error bar, except the C19—C24 bond which equals 1.426 (5) and 1.394 (5) Å for the monoclinic and orthorhombic polymorphs. Thus, the tendency suggested here is a slight modulation of the delocalization parameter between the dioxolene and the iron ion for the molecules in (1) or (2) [a relatively larger Fe^{II} semiquinonate character for (2), at any temperature]. This electronic effect analysed through the [(TPA)Fe(*R*-Cat)](*X*) series (*R* = various substituent, *X* = anion) was shown to modify the visible absorption spectra (Enachescu *et al.*, 2006), as the latter are dominated by strong ligand-to-metal charge-transfer transitions both in the high-spin and low-spin states (Simaan *et al.*, 2005). The DFT calculations and experimental studies of the EPR spectrometries of the Fe^{III} catecholate complexes (Girerd *et al.*, 2008) have established that these Fe^{III} catecholate compounds show a rather strong electronic delocalization between the dioxolene and the metal ion. The wavefunction was then discussed as a linear combination of two wavefunctions associated with the Fe^{III}Cat and Fe^{II}SQ configurations: $\Psi = \lambda\Psi_{Fe(II)SQ} + (1-\lambda^2)^{0.5}\Psi_{Fe(III)Cat}$. The *g* factors values obtained for Fe^{III}-TCC compounds, which are the λ^2 and $(1-\lambda^2)$ weighted contributions of Fe^{III}Cat and Fe^{II}SQ in this model, were found to be consistent with the data [monoclinic 2.112 (λ = 0.75); orthorhombic 2.15 (λ = 0.57); solution 2.145 (λ = 0.66)]. Spectral changes owing to the oxidation of Fe^{III} catecholate into Fe^{III} semiquinonate were also observed in solution by spectroelectrochemistry (Dei *et al.*, 1993). Accordingly, the optical properties related to the electronic delocalization within the Fe^{III} dioxolene moiety might differ between the two polymorphs.

Structural differences between the polymorphs come from the molecular packing (Fig. 5). Both crystalline structures consist of $[(TPA)Fe(TCC)]^+$ and PF_6^- (*ac*) layers alternating along the crystalline *b* axis. The structure of the cation layer is similar in both polymorphs with a π-stacking-type molecular

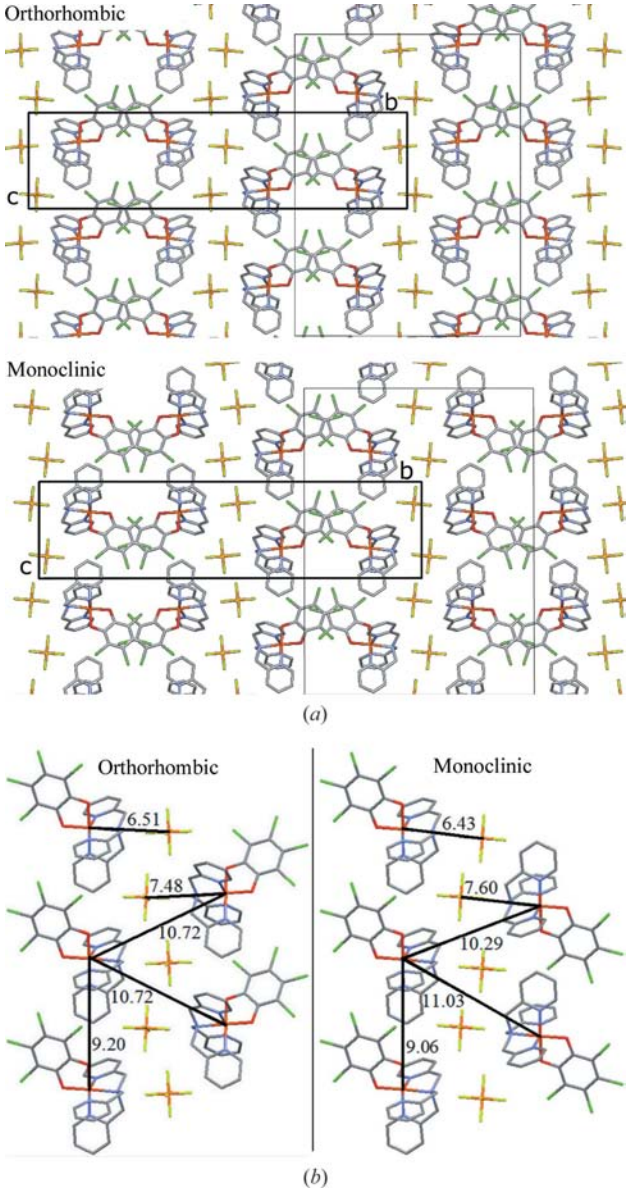

Figure 5
(*a*) Molecular packing in the *bc* plane for the orthorhombic and monoclinic polymorphs. *b* is horizontal and *c* is vertical. (*b*) Enlargement showing the interlayer packing in these *bc* planes with the different interlayer distances (error bars are less than 0.01 Å).

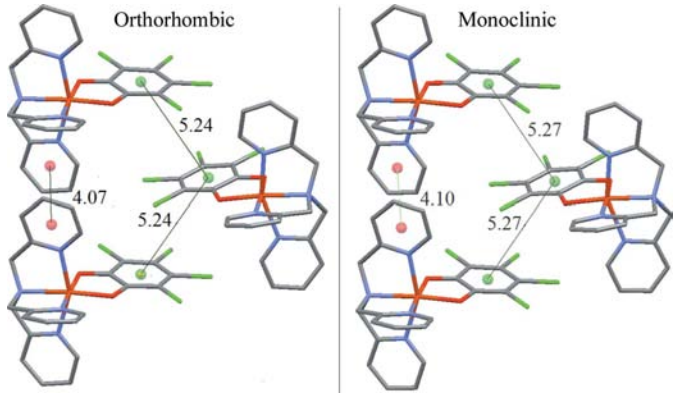

Figure 6
π stacking for both polymorphs in the cation layer. The distances between the centroids (red sphere) of the TPA cycles and of the TCC cycles (green sphere) differ slightly in the two compounds (error bars are less than 0.01 Å).

packing. This feature is quite unique in view of the published structures of polymorphism of other spin-crossover systems, the origin of which was mainly associated with distinct molecular packing. Nevertheless, characteristic distances between the TCC and TPA cycles slightly differ owing to the relative variations of the lattice parameters a and c, and also to the β angle, which is different from 90° in the monoclinic polymorph (Fig. 6). The anion layer packing is also similar in both polymorphs (Fig. 7), and the lower symmetry of the monoclinic systems gives four different first-neighbour distances (two for the orthorhombic). The anion–anion distances differ with average values of 6.45 Å (orthorhombic) and 6.42 Å (monoclinic). A stronger disorder of the anion in the orthorhombic system can be seen, characterized by larger displacement ellipsoids (Fig. 7). The major variation is the inter-layer packing (Fig. 5). The orthorhombic polymorph is noncentrosymmetric and all the cations are oriented in the same direction with the TCC pointing one way along c, because of the $Pna2_1$ space group. This is not the case for the monoclinic polymorph, which possesses inversion symmetry and for which layers alternate with top-to-bottom orientation of the TCC. Consequently, the interactions between the $[(TPA)Fe(TCC)]^+$ cation and PF_6^- anion layers are also dissimilar (Fig. 5).

Therefore, the optical properties of (1) and (2) (Figs. 2 and 4) presented in §3.2 may originate from the slightly different molecular structures and related electronic distribution. In addition, the specific molecular packing may also modify the band structures in the two solids as it modifies for example the amplitude of the transfer integral associated with π-stacking.

3.4. Spin crossover

As the temperature decreases the unit-cell volume shrinks (Fig. 8). It is not only due to thermal contraction, but it is mainly associated with the thermal conversion to the LS state around the $T_{1/2}$ and the concurrent Fe—L bond contraction which causes a decrease in molecular volume. The thermal conversion between two polymorphs is shifted by $\sim$11 K, which agrees well with magnetic data (Fig. 2). These observations are consistent with our previous investigation of Fe^{III} catecholate complexes (Floquet *et al.*, 2005). The latter suggests that the magnetic properties are mainly influenced by changes in the unit-cell volume *via* the effective environmental pressure (chemical pressure) experienced by the spin-crossover unit. The polymorph with the larger unit-cell volume at any temperature – orthorhombic solid – exhibits a spin crossover shifted to a lower temperature. Differences observed either at the molecular level, or in the intralayer packing, are thus not significant enough to measurably affect the spin-crossover of the two solids. This feature was also mentioned (Floquet *et al.*, 2005) for the [(TPA)Fe(R-Cat)]X series. It strongly contrasts with the case of iron(II) Fe-(PM-BIA)$_2$(NCS)$_2$ polymorphs, which show crossover-type or pronounced first-order thermal conversion (Marchivie *et al.*, 2003). It is well known that intermolecular coupling plays a key role in the cooperativity which may exist between molecules in the solids. If strong, such coupling can drive a first-order transition. If not, molecules behave in a more-or-less independent way approaching the thermal response of independent molecules in solution.

To describe the microscopic origin of the thermal spin conversion, the Wajnflasz model was used (Nishino *et al.*, 2003; Boukheddaden *et al.*, 2005). It is similar to the Ising model, where the total Hamiltonian depends on the spin state of the ith molecule S_i constituting the system ($S_i < 0$ for the LS state and $S_i > 0$ for the HS state). At the molecular level, the energy difference Δ between the HS and LS states and the ratio g between the degeneracy of HS and LS states are the driving parameters. Δ is related to the ligand field surrounding the Fe atoms (an intramolecular contribution, and a work term $p\Delta V$ due to the effective environmental pressure). From the above discussion, we can conclude that Δ should be slightly different for the two polymorphs since the intramolecular environments are not exactly the same (Fig. 4). Cooperativity is strongly associated with the intermolecular interactions. The Hamiltonian used in the nearest-neighbour approximation has an

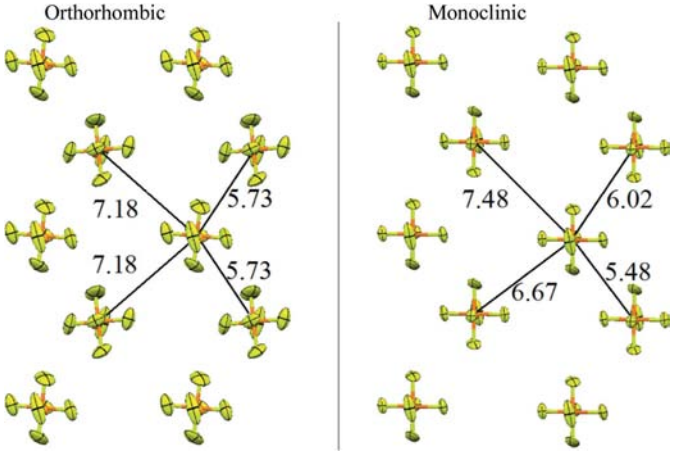

Figure 7
Anion packing in the *ac* plane for the orthorhombic and monoclinic polymorphs. Ellipsoids are shown at the 50% probability level for the structure at 80 K (error bars are less than 0.01 Å).

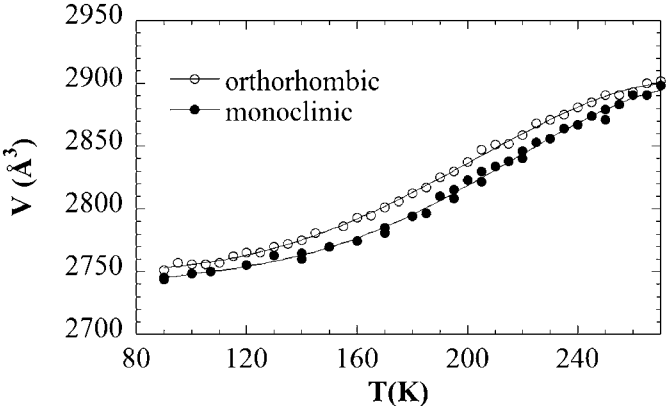

Figure 8
Temperature dependence of the unit-cell volume of both polymorphs around the crossover.

additional driving parameter through the coupling constant J (mainly of elastic nature). The Hamiltonian then takes the following form

$$H = -J \sum_{<i,j>} S_i S_j - h \sum_i S_i, \text{ with } h = -\Delta + kT \ln(g)/2, \quad (2)$$

where h represents the effective field surrounding the molecules. If the intermolecular coupling is strong enough, a first-order phase transition occurs, and if not, a crossover takes place instead.

In the presently discussed case of the $[(TPA)Fe(TCC)]PF_6$ polymorphs, the observation of a crossover in each shows that both systems are weakly cooperative, with the characteristic temperature $T_{1/2}$ shifted by only ~ 11 K. In view of the present crystallographic study, we can conclude that the intralayer cation–cation couplings are similar in both polymorphs, because of the similar structure of the cation layers (packing and distances). In addition, the interlayer cation interaction is screened through the intercalated PF_6^- anion layers in each of the polymorphs. The elastic interactions are then mainly intralayer in nature and the crossover behaviour rather than the first-order transition observed in orthorhombic and monoclinic forms is then directly related to the insufficient strength of these interactions.

4. Conclusion

We have identified two polymorphs of $[(TPA)Fe(TCC)]PF_6$, which undergo thermal spin crossover. Significant structural signatures are associated with the thermal spin-conversion both at the intra- or intermolecular levels. The analysis reveals a unique feature that polymorphism is feasible through packing differently similar anion and cation layers. The slight shift between the polymorphs during the thermal spin crossover, rather unusual for this family of materials, results from the similar intralayer structure leading to similar cation–cation interactions, as discussed within the Ising-like model.

This work was supported by the Institut Universitaire de France, the Ministry of Research of France (ACI JC E. Collet, ANR 'Fast-switch' NT05-3_45333, NOE MAGMANet (515767–2), Région Bretagne (CREATE Ultimate 4146, PRIR Femtocom 2178, SIE MagBreiz 2142, PhD funding of JH) and Rennes Métropole.

References

Altomare, A., Burla, M. C., Camalli, M., Cascarano, G. L., Giacovazzo, C., Guagliardi, A., Moliterni, A. G. G., Polidori, G. & Spagna, R. (1999). *J. Appl. Cryst.* **32**, 115–119.

Boone, S. R., Purser, G. H., Chang, H. R., Lowery, M. D., Hendrickson, D. N. & Pierpont, C. G. (1989). *J. Am. Chem. Soc.* **111**, 2292–2299.

Boukheddaden, K., Nishino, M., Miyashita, S. & Varret, F. (2005). *Phys. Rev. B*, **72**, 014467.

Collet, E., Buron-Le Cointe, M., Lorenc, M. & Cailleau, H. (2008). *Z. Kristallogr.* **223**, 272–282.

Dei, A., Gatteschi, D. & Pardi, L. (1993). *Inorg. Chem.* **32**, 1389–1395.

Duriska, M. B., Neville, S. M., Moubaraki, B., Cashion, J. D., Halder, G. J., Chapman, K. W., Balde, C., Létard, J. F., Murray, K. S., Kepert, K. J. & Batten, S. R. (2009). *Angew. Chem. Int. Ed.* **48**, 2549–2552.

Enachescu, C., Hauser, A., Girerd, J.-J. & Boillot, M.-L. (2006). *Chem. Phys. Chem.* **7**, 1127–1135.

Farrugia, L. J. (1997). *J. Appl. Cryst.* **30**, 565.

Floquet, S., Simaan, A. J., Rivière, E., Nierlich, M., Thuéry, P., Ensling, J., Gütlich, P., Girerd, J.-J. & Boillot, M.-L. (2005). *Dalton Trans.* pp. 1734–1742.

Girerd, J.-J., Boillot, M.-L., Blain, G. & Rivière, E. (2008). *Inorg. Chim. Acta*, **361**, 4012–4016.

Glijer, D., Hébert, J., Trzop, E., Collet, E., Toupet, L., Cailleau, H., Matouzenko, G. S., Lazar, H. Z., Létard, J. F., Koshihara, S. & Buron-Le Cointe, M. (2008). *Phys. Rev. B*, 134112.

Guionneau, P., Marchivie, M., Bravic, G., Létard, J.-F. & Chasseau, D. (2004). *Top. Curr. Chem.* **234**, 97–128.

Gütlich, P. & Goodwin, H. A. (2004). Editors. *Spin Crossover in Transition Metal Compounds*, Vols. 233, 234, 235. New York: Springer.

Jang, H. G., Cox, D. D. & Que, L. (1991). *J. Am. Chem. Soc.* **113**, 9200–9204.

Jo, D. H. & Que, L. (2000). *Angew. Chem. Int. Ed.* **39**, 4284–4287.

Johnson, C. K. (1965). *ORTEP*, Report ORNL-3794. Oak Ridge National Laboratory, Tennessee, USA.

Koch, W. O., Schunemann, V., Gerdan, M., Trautwein, A. X. & Kruger, H.-J. (1998). *Chem. Eur. J.* **4**, 1255–1265.

Koningsbruggen, P. J., Maeda, Y. & Oshio, H. (2004). *Top. Curr. Chem.* **233**, 259–324.

Létard, J.-F., Chastenet, G., Nguyen, O., Marcén, S., Marchivie, M., Guionneau, P., Chasseau, D. & Gütlich, P. (2003). *Monatsh. Chem.* **134**, 165–182.

Létard, J.-F., Guionneau, P., Rabardel, L., Howard, J. A. K., Goeta, A., Chasseau, D. & Kahn, O. (1998). *Inorg. Chem.* **37**, 4432–4441.

Marchivie, M., Guionneau, P., Létard, J.-F. & Chasseau, D. (2003). *Acta Cryst.* B**59**, 479–486.

Matouzenko, G. S., Bousseksou, A., Lecocq, S., Van Koningsbruggen, P. J., Perrin, M., Kahn, O. & Collet, A. (1997). *Inorg. Chem.* **36**, 5869–5879.

Mitra, S., Raston, C. L. & White, A. H. (1978). *Aust. J. Chem.* **31**, 547.

Moisan, N., Servol, M., Lorenc, M., Tissot, A., Boillot, M.-L., Cailleau, H., Koshihara, S. & Collet, E. (2008). *C. R. Chim.* **11**, 1235–1240.

Nishino, M., Boukheddaden, K., Myashita, S. & Varret, F. (2003). *Phys. Rev. B*, **68**, 224402.

Oxford Diffraction (2008*a*). *CrysAlis CCD*, Version 1.171.26. Oxford Diffraction Ltd, Abingdon, Oxfordshire, England.

Oxford Diffraction (2008*b*). *CrysAlis RED*, Version 1.171.26. Oxford Diffraction Ltd, Abingdon, Oxfordshire, England.

Peresypkina, E. V., Bushuev, M. B., Virovets, A. V., Krivopalov, V. P., Lavrenova, L. G. & Larionov, S. V. (2005). *Acta Cryst.* B**61**, 164–173.

Pillet, S., Legrand, V., Weber, H. P., Souhassou, M., Létard, J.-F., Guionneau, P. & Lecomte, C. (2008). *Z. Kristallogr.* **223**, 235–249.

Reger, D. L., Gardinier, J. R., Smith, M. D., Shahin, A. M., Long, G. J., Rebbouh, L. & Grandjean, F. (2005). *Inorg. Chem.* **44**, 1852–1866.

Sheldrick, G. M. (2008). *Acta Cryst.* A**64**, 112–122.

Sheu, C. F., Pillet, S., Lin, Y. C., Chen, S. M., Hsu, I. J., Lecomte, C. & Wang, Y. (2008). *Inorg. Chem.* **47**, 10866–10874.

Spek, A. L. (2009). *Acta Cryst.* D**65**, 148–155.

Simaan, A. J., Boillot, M.-L., Carrasco, R., Cano, J., Girerd, J.-J., Mattioli, T. A., Ensling, J., Spiering, H. & Gütlich, P. (2005). *Chem. Eur. J.* **11**, 1779–1793.

Thompson, A. L., Goeta, A. E., Real, J. A., Galet, A. & Muñoz, M. C. (2004). *Chem. Commun.* pp. 1390–1391.

Yu, L. (2002). *J. Phys. Chem. A*, **106**, 544–550.